AIAA 81-0067R

Theoretical and Experimental Analysis of the Flow through Supersonic Compressor Rotors

K.-D. Broichhausen* and H. E. Gallus†
Technical University Aachen, Aachen, West Germany

In the present paper theoretical and experimental results referring to different supersonic rotors are discussed. The theoretical approach, based on the Euler equations of motion, is valid for transonic rotor flows. The shocks are treated separately on the basis of the Rankine-Hugoniot equations. The measurements were performed by time-averaging and time-dependent techniques. Comparing the theoretical approach with the experimental data, special attention is paid to the structure of detached front waves and strong channel shocks. These discontinuity surfaces proved to be remarkably spatially curved, so that the pressure rise in the shocks is lower than in the two-dimensional case. With respect to the channel and the rotor outlet flow the presented theoretical results conform to the experimental data, if three-dimensional viscous effects are not dominant.

Nomenclature

a	= velocity of sound
c,u,w	= absolute, circumferential, and relative velocity
c_v	= specific heat
d( )/ds	= differential change in streamline direction
dl	= increment in streamline direction (r, z plane)
f_{blade}	= blade force
h_{rot}	= rothalpy
M_{rel}, M_z	= relative, axial Mach number
$n_{(e)}$	= normal (unity) vector
n/n_0	= speed ratio
$p_{(t)}, T_{(t)}$	= (total) pressure, (total) temperature
$\bar{p}$	= time dependent pressure
Q	= arbitrary variable
r	= radius
rdϑ	= increment in circumferential direction
R	= gas constant, $= c_p - c_v$
s	= entropy
S	= finite area
x,y	= profile coordinates
(d)z	= (increment in) axial direction
α	= Mach angle
Γ	= circulation
γ,φ,λ	= flow angle in r-z; r-rϑ plane, $S1$ surface
ϵ	= blade angle
$\Delta^{i,k}Q$	= central difference in i, k direction
κ	= ratio of specific heats
$\rho_{(t)}$	= (total) density
σ	= three-dimensional shock angle
ω	= angular velocity
Ω	= vorticity

Subscripts

abs, rel	= absolute, relative system
i,j,k	= grid point
u,r,z	= circumferential, radial, axial
l	= streamline (r, z plane)
$S1$, $S2$	= $S1$, $S2$ surface
sh	= shock
son	= sonic
0	= total
1,2	= upstream/downstream
| |	= magnitude of vector

Presented as Paper 81-0067 at the AIAA 19th Aerospace Sciences Meeting, St. Louis, Mo., Jan. 12-15, 1981; submitted Feb. 19, 1981; revision received Sept. 14, 1981.

*Research Engineer, Institute for Jet Propulsion and Turbomachines.

†Professor, Institute for Jet Propulsion and Turbomachines.

I. Introduction

ONE aim of the development of axial flow compressors, among others, is an increase of the specific power of single stages. To correspond to these efforts, efficient transonic compressor stages were constructed. A further power concentration is possible by means of supersonic compressors. A one-dimensional stage design considering the losses[1] shows that two concepts of supersonic compressor stages are expedient. The stages are equipped with tandem stators; their rotors, however, are of a different type, i.e., an impulse-type rotor or a shock-in-rotor-type rotor (Fig. 1). In the impulse-type rotor the supersonic relative flow is turned in the axial direction, with constant respectively increasing relative velocity. Such a rotor was designed in Ref. 2 by a quasi-three-dimensional method of characteristics and was investigated experimentally.

In contrast to the impulse-type rotor, the shock rotors contribute to the increase of the static pressure, since at the entrance of these rotors a strong shock is stabilized slowing down the supersonic relative velocity to subsonic speeds. The stabilization of this shock can be realized by back pressure or by a diminution of the rotor channel cross-sectional area.

The calculation of the complex flow in such rotors must cover the three-dimensional, rotational, transonic flow through rotor channels with high turning. This is possible either by means of a time-marching method[3-7] or by a method based on the equation of motion for stationary flow,[8-11] with a separate treatment of the shocks. The latter methods also include the numerical technique which is discussed in the present contribution and the results of which are compared with experimental data from the rotors outlined in Fig. 1.

II. Quasi-Three-Dimensional Calculation of Flow in Supersonic Rotors with Strong Shocks and Extended Subsonic Regions

Basic Equations

The calculation presumes an ideal gas and frictionless flow and is made on the basis of the continuity equation, the equation of motion, and the energy equation referring to the rotor flow. The rotation of the absolute flow is defined as

$$2\Omega = \nabla \times c \tag{1}$$

From these basic equations a further relation results which corresponds to Crocco's law for a stationary reference system.

$$2(w\times\Omega)=\nabla h_{\text{rot}}-T\nabla s \tag{2}$$

The Stokes theorem combines the rotation of the absolute flow and the circulation Γ, which is defined as a line integral of the velocity along a closed curve.

$$\Gamma=\int d\boldsymbol{r}\cdot\boldsymbol{c}=2\iint\Omega\cdot\boldsymbol{n}dS \tag{3}$$

Since the circulation along the streamline is constant, a combination of Eqs. (2) and (3) results in a further conservation law, which is applied to the computation of the rotational flow.

The calculation itself is a quasi-three-dimensional approach.[12] It is made on blade-to-blade stream surfaces (*S1*) and on *S2* surfaces extending from hub to tip. The common tangent of both surfaces follows the direction of a relative velocity vector. Consequently, the computation may involve an additional condition, according to which the normal vector of the surfaces is perpendicular to the relative velocity.

In a real rotor flow both stream surfaces are spatially curved. The problem is simplified with sufficient accuracy, especially in the case of axial turbomachines, if the *S1* surfaces are assumed to be rotational symmetric. This assumption allows the computation of the flow by solving the fundamental equations in a coordinate system aligned on the rotational symmetric *S1* surfaces. The conversion of a given variable Q between the cylindrical coordinates and the system aligned with the *S1* surfaces can be made by means of the following transformation (Fig. 2):

$$n_{S1}\frac{\partial Q}{\partial l}=n_{S1,r}\frac{\partial Q}{\partial z}+n_{S1,z}\frac{\partial Q}{\partial r} \tag{4}$$

The normal vector n_{S1} necessary for this conversion can be established by the geometry of the stream surface.

Method of Characteristics in Supersonic Regions

Due to relative supersonic velocity and a subsonic axial component the curved front waves of the blades running upstream generate an entropy gradient already in the inlet flowfield of the rotor (Fig. 1). Therefore, the numerical procedure consists of a method of characteristics for strongly curved profiles considering the rotation Ω. The basic equations are the components of the continuity equation and the equation of motion for the steady relative flow. These relations and the corresponding thermodynamic laws lead to a system of differential equations for the computation of the *S1* surface flow. This system can be formulated in matrix notation

$$C_i=A_{i,j}\cdot B_j \tag{5}$$

The structure of the single elements can be seen in the Appendix.

The characteristics of this equation system define three distinct directions. The first characteristic direction is determined by the streamline, since part of the equations corresponds to the Euler equation along a relative streamline. In addition, two further characteristic equations result. The structure of the latter resembles that of the right- and left-running characteristics of the two-dimensional flow.

In a cylindrical coordinate system (Fig. 3) the following slope condition and compatibility relation result for the *S1* surface:

$$\frac{r\,d\vartheta}{dl}=\tan(\lambda\pm\alpha) \tag{6}$$

$$\begin{aligned}dw=&\pm w\,d\lambda\tan\alpha-\frac{w\sin^2\alpha}{\kappa R}ds+\frac{\omega^2 r}{w}dr\pm w\,dl\tan\alpha\frac{\sin\gamma}{r}\\&\times\left\{\tan(\lambda\pm\alpha)\left(\sin\lambda+\frac{u}{w}\right)^2+\cos\lambda\left(\sin\lambda-2\frac{u}{w}\right)\right\}\\&\pm w\,dl\tan\alpha\cos\lambda(\cos\lambda\tan(\lambda\pm\alpha)-\sin\lambda)\cos\gamma H_s\\&-\left(\frac{1}{\rho}H_\rho+\frac{1}{\kappa}H_s\right)dr\end{aligned} \tag{7}$$

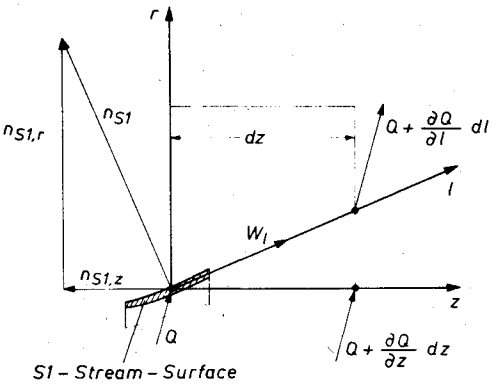

Fig. 2 *S1* **stream surface transformation.**

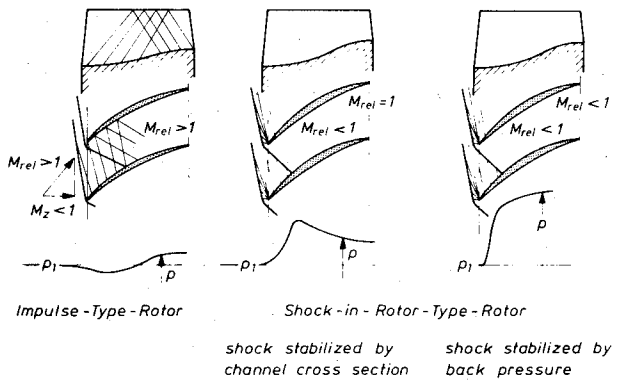

Fig. 1 Supersonic rotors.

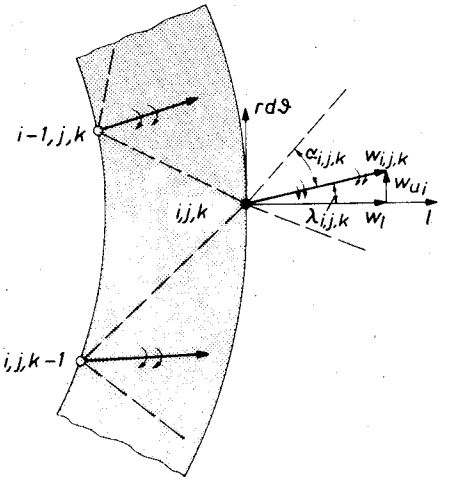

Fig. 3 Characteristics of the rotational *S1* surface.

In the present case of a rotational relative flow the third characteristic in the streamline direction is decisive for the entropy distribution. As the entropy is constant along a streamline, it is dependent directly on the streamline function.

Thus, in case of a given entropy distribution behind the front wave, the entropy in the grid points of the supersonic region can be determined with the aid of the stream function by numerical interpolation

$$s_{i,k}=\frac{\Delta^i s}{2\Delta^i\psi}\{2\psi_{i,k}-(\psi_{i-1,k}+\psi_{i,k-1})\}+\frac{s_{i-1,k}+s_{i,k-1}}{2} \quad (8)$$

Finite Area Integration in Subsonic Regions

In the present case of strongly curved thin blades the rotational subsonic flow is dealt with on the basis of the modified vorticity theorem for the relative flow, Eq. (2). The vorticity behind a strong shock causing subsonic velocity can be determined directly from the entropy gradient and the streamline geometry of a homogeneous inlet flow.

$$2\Omega=\begin{bmatrix} -\frac{1}{w_z}T\frac{\partial s}{r\partial\vartheta}+\frac{2w_r}{w_z}\Omega_z-f_{\text{blade}} \\ -\frac{1}{w_u}T\frac{\partial s}{\partial r}+\frac{2w_z}{w_u}\Omega_u \\ \frac{\partial w_r}{\partial s}\frac{(1+\tan^2\gamma\sin^2\varphi)^{1/2}}{\sin\varphi}-\frac{\partial w_z}{\partial r}\end{bmatrix} \quad (9)$$

Since the normal vector of the rotational symmetric *S1* surface has no component in circumferential direction, the circulation of a finite grid area behind the shock becomes

$$\Gamma(l,r\mathrm{d}\vartheta)=2\iint(\Omega_z\sin\gamma+\Omega_r\cos\gamma)r\mathrm{d}\vartheta\mathrm{d}l \quad (10)$$

On the other hand, however, the circulation is also defined as a line integral of the absolute velocity along the boundaries of a finite grid element. For this integration a quasi-streamline grid is used, which is also generated in subsonic regions by means of the stream function.

If the components of the absolute velocity are replaced by relative and circumferential velocity, the integration around a finite grid area (Fig. 4) gives the following difference scheme with the aid of central differential approximation:

$$\Gamma_{i,j,k}=\Delta^k w\Delta^i s-u_i\Delta^k\cos\lambda\Delta^i s-(\Delta^i u+\Delta^i w_u)r\Delta^k\vartheta \quad (11)$$

Since the circulation of the stream filament under consideration is constant in the absence of shocks and can be determined at the upstream boundary of the area, the difference Eq. (11) indicates a velocity distribution.

The circulation at the upstream boundary of the subsonic region, however, is calculated by integration in a rectangular coordinate system, whereas a quasi-streamline grid is used within the subsonic parts. Therefore equalization of Eqs. (10) and (11) also requires a transformation of the surface integral

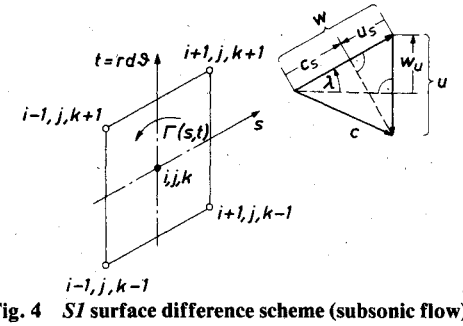

Fig. 4 *S1* surface difference scheme (subsonic flow).

by means of a functional determinant derived from the grid geometry of the two systems. Then the circulation of any grid element along a streamline, and the corresponding velocities at the boundaries of the element, can be determined from the circulation behind the strong compression shock. The applicaton of the energy and continuity equation results in the variables of state at the rotational subsonic flow on an *S1* surface.

Treatment of Shocks and Front Waves

The complex transonic rotor flow involves front waves and channel shocks. The theoretical treatment of these discontinuity surfaces takes into consideration 1) the asymmetric structure of the strong channel shocks and the front waves as well as 2) the three-dimensional structure of the compression shocks. First all parts of channel shock and front wave with subsonic downstream velocities are described by a hyperbolic model (Fig. 5), which has been modified in comparison to Ref. 13.

Considering the shock geometry and the gasdynamic relations of the detached shock, one obtains for the shock detachment distance L a relation of the form

$$L_{S,CP,CS}=L\left\{y_0,y_{\text{son-blade}},\alpha,\sigma_{\text{son}},\zeta,\left(\frac{A_1}{A_{\text{son}}}\right)_{\Delta s=0}\frac{p_{0\text{-son}}}{p_{0\text{-}1}}\right\} \quad (12)$$

A coupling of the different subsonic parts of the front wave results in an influence of the channel flow on the suction side front wave S and in a slight deviation of the stagnation streamline.

The parts of the shock with supersonic downstream velocity are fitted by means of a calculation according to the method of characteristics and the Rankine-Hugoniot equations.

Since the shock surfaces under consideration are spatially curved, a calculation of the shock must take into account the spatial shock angles. For this purpose the three-dimensional shock front is determined by the angles γ_{sh} and φ_{sh} and described by its normal vector (Fig. 6).

$$n_{\text{sh}}=\begin{bmatrix}-\sin\varphi_{\text{sh}}\cdot\cos\gamma_{\text{sh}} \\ -\cos\varphi_{\text{sh}}\cdot\cos\gamma_{\text{sh}} \\ \cos\varphi_{\text{sh}}\cdot\sin\gamma_{\text{sh}}\end{bmatrix} \quad (13)$$

Then the spatial shock angle decisive for an exact calculation ensues from the following relation:

$$\sigma_{\text{sh}}=\arcsin\frac{w\cdot n_{\text{sh}}}{|w|\,|n_{\text{sh}}|} \quad (14)$$

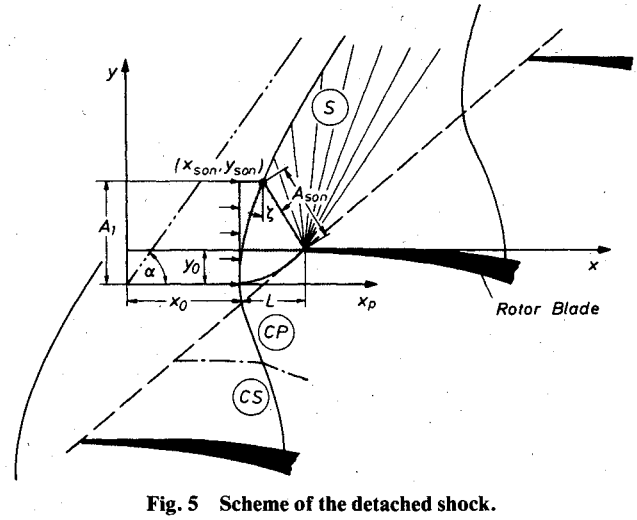

Fig. 5 Scheme of the detached shock.

Calculation on the *S2* Surfaces

In connection with the present equation system it is convenient to compose the flow derivatives along an *S2* surface by the radial and circumferential gradients and the corresponding relations. The gradients of density and velocity necessary for this composition can be determined from the flow properties on an *S1* surface by means of the basic flow equations.

$$\frac{1}{\rho}\frac{\partial \rho}{r\partial \vartheta} = -\frac{1}{a_t^2}\left(\frac{\rho_t}{\rho}\right)^{\kappa-1}\left\{\frac{w_r}{r}(w_u+2u)+w\frac{\mathrm{d}w_u}{\mathrm{d}s}\right\}+\frac{\kappa-1}{a_t^2\cdot\rho_t}\frac{p_t}{r\partial\vartheta} \tag{15}$$

$$\frac{1}{\rho}\frac{\partial \rho}{\partial r} = \frac{1}{a_t^2}\left(\frac{\rho_t}{\rho}\right)^{\kappa-1}\left\{\omega^2 r - w\frac{\partial w_r}{\partial r}\right\}+\frac{1}{p_t}\frac{\partial p_t}{\partial r}$$

$$w\frac{\partial w}{r\partial\vartheta} = \frac{1}{\rho}\frac{\partial p_t}{r\partial\vartheta}\frac{p}{p_t}+\frac{w_r w_u}{r}+2\omega w_r + w\frac{\mathrm{d}w_u}{\mathrm{d}s}$$

$$w\frac{\partial w}{\partial r} = \frac{1}{\rho}\frac{\partial p_t}{\partial r}\frac{p}{p_t}-\left(2\omega w_u+\frac{w_u^2}{r}\right)\left(1-\frac{w_r}{w_u}r\frac{\partial \epsilon}{\partial r}\right)+w\frac{\mathrm{d}w_r}{\mathrm{d}s} \tag{16}$$

The *S2* surface gradient of a variable Q results from the transformation equation of the quasi-three-dimensional approach (Fig. 7).

$$\frac{\partial Q}{\partial h} = \{1-(n_{e-S1}\cdot n_{e-S2})\}^{1/2}\frac{\partial Q}{\partial r}+(n_{e-S1}\cdot n_{e-S2})\frac{\partial Q}{r\partial\vartheta} \tag{17}$$

with

$$n_{e-S1} = \frac{n_{S1-r}}{|n_{S1-r}|};\quad n_{e-S2} = \frac{n_{S2-r/r\mathrm{d}\vartheta}}{|n_{S2-r/r\mathrm{d}\vartheta}|}$$

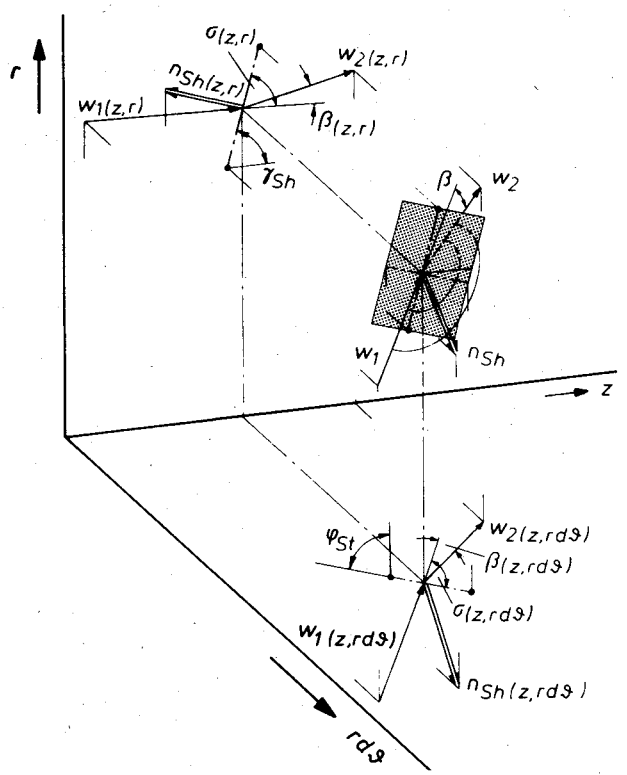

Fig. 6 Three-dimensional structure of compression shocks.

The numerical procedure downstream of strong shocks follows Fig. 8a. From the given flow properties along a stream-surface j one can derive the flow conditions and the slope of the neighboring stream surface $j-1$ in the grid points i', k, and $i'+1$, k. As the shock front normally is inclined in the r, z plane, the required data downstream of the shock (grid point i, k) are calculated by extrapolation of the streamline shape and the flow properties. Then the shock itself is fitted iteratively between subsonic and supersonic regions under consideration of three-dimensional effects. Within the subsonic region the calculation of the flow properties of a neighboring *S2* surface follows Fig. 8b. The shape of the *S2* surface itself is determined by numerical mass flow integration in the radial direction.

III. Theoretical and Experimental Results

Wall Pressure Distribution

The experimental investigations of the described rotors (Fig. 1) are conducted in a compressor test rig which is presented in detail in Refs. 2, 14, and 15. In addition to these investigations, further information about the flow in

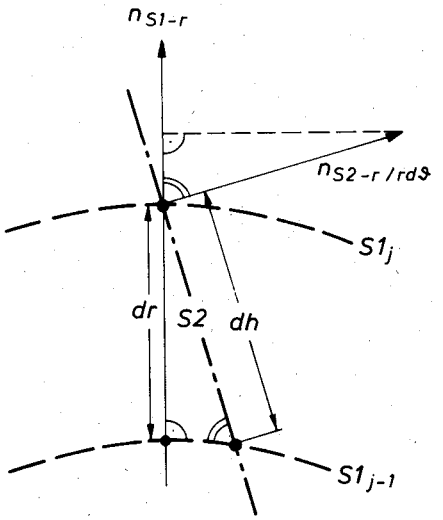

Fig. 7 *S2* surface calculation.

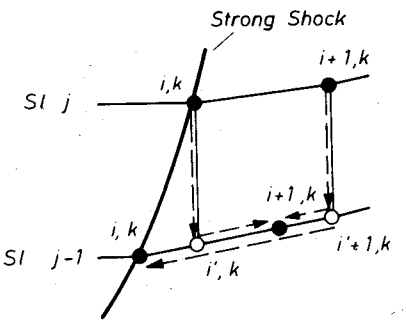

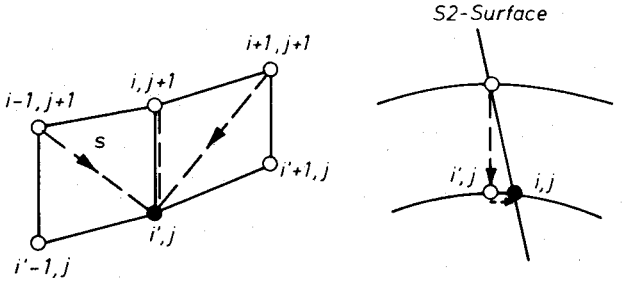

Fig. 8 *S2* surface grid.

supersonic rotors is given by the investigation of the rotor with shock stabilization by channel cross section. The measured wall-pressure distributions at overspeeds (Fig. 9) show that, with increases in speed, the intensity of the shock-conditioned pressure increase in the entrance region sharply decreases, and the position of the pressure maximum shifts in the axial direction. Such remarkable changes of position and intensity of the channel shock appear if the front wave attaches to the rotor leading edge and the downstream velocity of the channel shock changes from subsonic to supersonic velocities. Consequently, no blockage effect occurs and a multishock system is generated in the rotor at overspeeds. However, increasing the back-pressure up to a static-pressure ratio of about 2 stalled all investigated rotors.

The back pressure of the rotor with the cross section stabilized shock, contrary to the other investigated rotors,[2,14] could not be increased to such an extent that it generated a stronger channel shock at the rotor entrance. Such a high back pressure involves too large a detachment of the frontwave at the hub and, consequently, a stalling of the rotor due to the three-dimensional equilibrium behind the channel shock. Figure 10 shows the wall pressure distributions for this rotor resulting from the design and the calculations for the measured back pressures under throttled and unthrottled conditions. Both experiment and calculation reveal that the pressure ratio realizable in the strong three-dimensional shock front is about 30% lower than the pressure rise in a straight compression shock. Though the shock front is stabilized by a critical cross section within the rotor, this sonic area is not positioned at the rotor exit, as provided by the design.

Entrance Flowfield

In the case of all investigated rotors the measurements showed a linear distribution of the relative Mach number ($M_{1\text{rel-hub}} \simeq 1.25 \ldots M_{1\text{rel-casing}} \simeq 1.58$) and the relative flow angle ($\beta_{1\text{-hub}} \simeq 147$ deg$\ldots\beta_{1\text{-casing}} \simeq 155$ deg). The measured data correspond to the design, which determines the mass flow because of the hyperbolic character of the front waves in accordance with the unique incidence condition. The theoretical approach, however, allows a nonuniform distribution of the flow conditions in the short range upstream of the rotor blading.

This nonuniform distribution in the entrance is shown by the measurements of the spatial unsteady pressure distribution upstream of the rotors (Figs. 11 and 13). The measurements were conducted by the semiconductor probe described in Ref. 15. The calculation of the front wave pattern upstream of the impulse-type rotor (Fig. 11) is based on the exit pressure measured in stage operation. The curved shape of the intersection line of the front wave and the axial measuring plane can be explained as follows.

In the hub region of this supersonic rotor a strong shock is generated with subsonic downstream velocity by the throttling effect of the stator. The radial equilibrium allows weak shocks only near the casing. This results from Fig. 12, where the course of the shock angle and the Mach numbers behind the shock are plotted as a function of the radius. In this figure, the results of the calculations are shown for stage

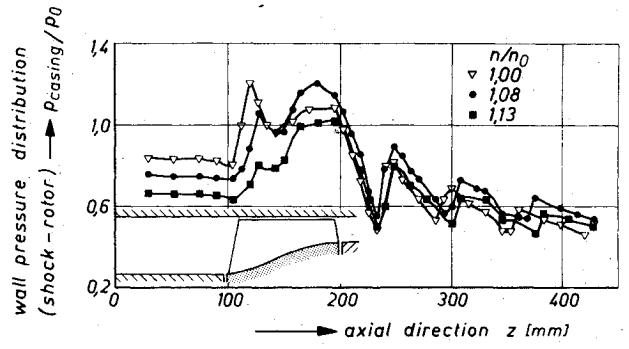

Fig. 9 Wall pressure distributions at overspeeds (rotor with cross-section stabilized shock).

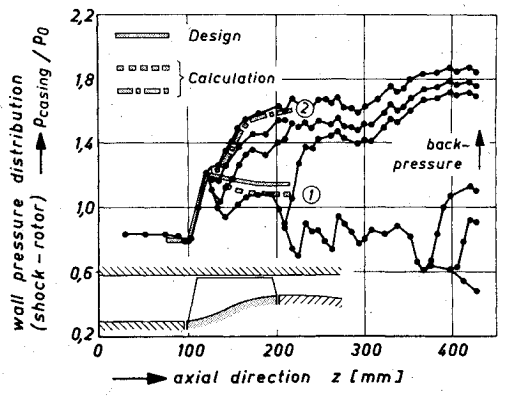

Fig. 10 Wall pressure distributions with back pressure (rotor with cross-section stabilized shock), ① unthrottled and ② throttled conditions.

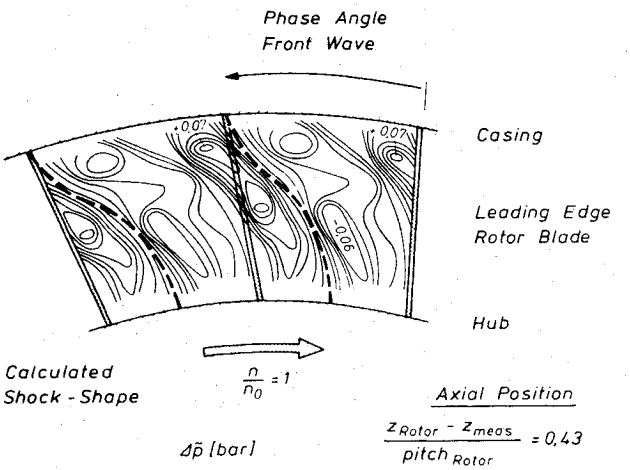

Fig. 11 Unsteady static pressure distribution upstream of the impulse-type rotor.

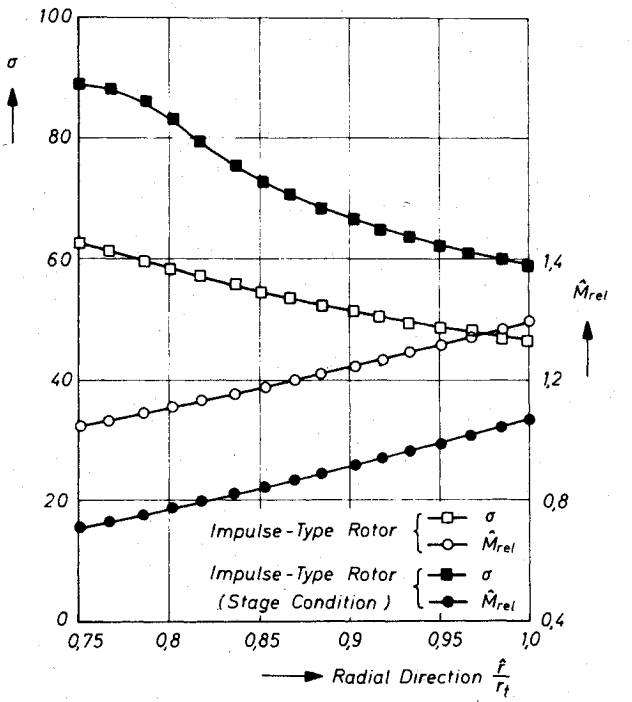

Fig. 12 Channel shocks in the impulse-type rotor.

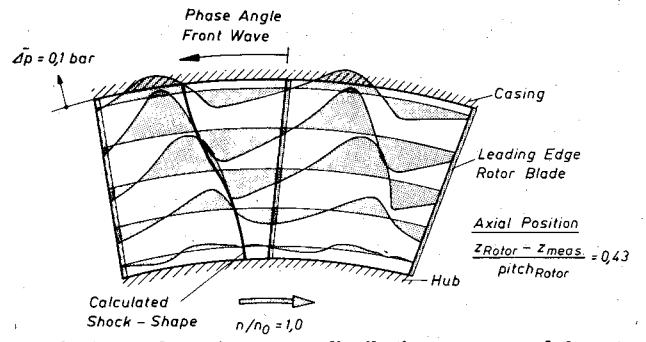

Fig. 13 Unsteady static pressure distribution upstream of the rotor with cross-section stabilized shock.

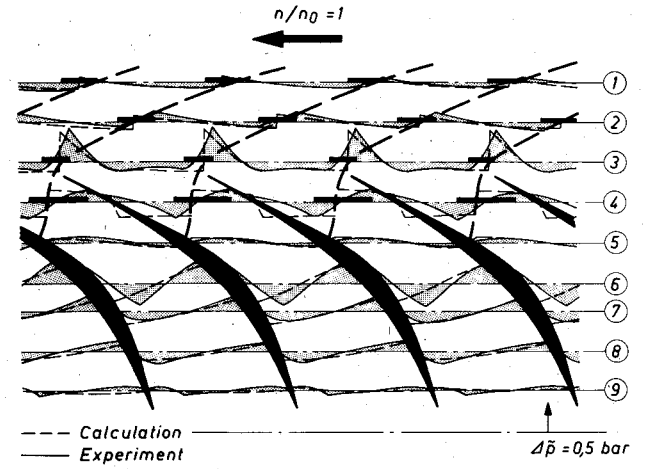

Fig. 14 Quasi-steady pressure distribution of the rotor with cross-section stabilized shock.

operation and operation without stator. Also, as the experiments confirm,[14] the rotor is throttled because of the higher back pressure in the stage. At the hub, this effect causes a strong shock with extensive subsonic regions.

A comparison of the data for the impulse-type rotor (Fig. 11) and the static pressure pulsations upstream of the shock rotor (Fig. 13) shows that the unsteady amplitudes are greater in the incidence flow of the shock rotor. These amplitudes, as well as the smaller phase angle in Fig. 13 between rotor leading edge and the shock, indicate a stronger detachment of the front wave. Furthermore, the shock front is less curved in this case, since there is no region with supersonic flow.

Channel Flow

Figure 14 shows a comparison of the calculated pressure gradients in the circumferential direction with the measuring result of the semiconductor transducers in the casing for the rotor with cross section stabilized shock. As can be seen from the static wall pressure distribution (Fig. 10), the front wave and the pressure distribution in the inlet flow, as well as the position of the channel shock and its intensity, confirm the presented theoretic model. Within the blade channel, too, the calculated pressure distribution in principle corresponds to the experiment. In the zone of suction-side separation, however, the numerical results show discrepancies. The inversion of the pressure gradient in the circumferential direction which occurs downstream of the shock and which is characteristic of rotors with strong entrance shocks is also covered by the computation.

Exit Flow

Figures 15 and 16 show the exit Mach numbers of the impulse-type rotor and the shock rotor resulting from computation and experiment. For the impulse-type rotor the experimental data[2] are compared with the presented

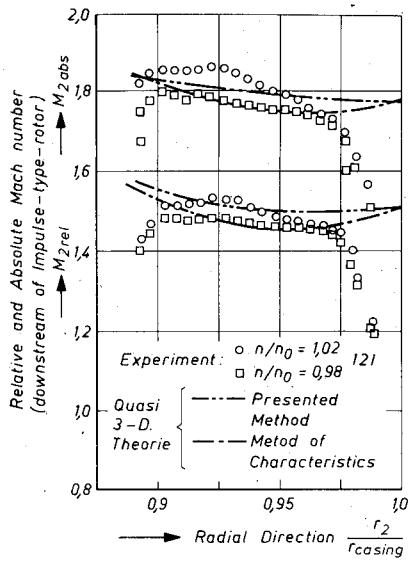

Fig. 15 Exit Mach numbers of the impulse-type rotor.

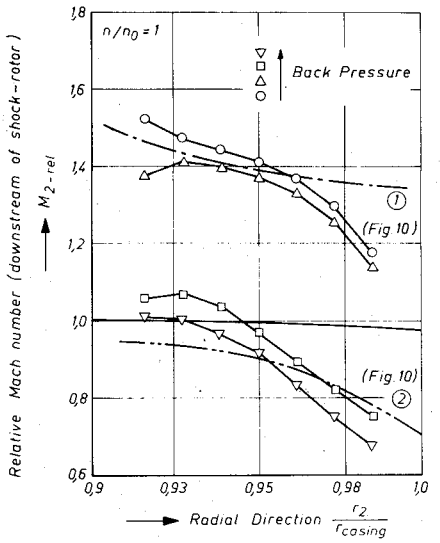

Fig. 16 Exit Mach numbers of the rotor with cross-section stabilized shock.

procedure and with the results of the method of characteristics[2] which considers subsonic zones by linear extrapolation. For the shock rotor in Fig. 16 different results of the calculation according to the wall-pressure distribution in Fig. 10 are compared. The graphs show that the exit Mach number of the rotor with a cross section stabilized shock is lower than that of the impulse-type rotor. It is, however, supersonic too. The difference between calculated and measured distribution is explained by viscous effects in the rear part of the blading.

IV. Conclusions

Theoretical and experimental results concerning three different rotors were discussed. The theoretical approach of three-dimensional flows through rotors with high turning of the blades proved to be in accordance with the measured data. Only in the case of strong viscous-inviscid interaction the results were less sufficient. The presented results also show 1) in the case of throttled rotors the three dimensionality of the shocks cause a lower pressure rise than predicted by a two-dimensional approach; and 2) in the case of blockage of the rotor flow caused by the channel geometry an increase of the speed does not result in stall conditions but to a diminution of the shock system.

Appendix: Elements of the Differential Equation System

$$A_{i,j}=\begin{bmatrix} \rho & 0 & 0 & \rho & w_l & w_u & 0 & 0 \\ dl & r d\vartheta & 0 & 0 & 0 & 0 & 0 & 0 \\ w_l & w_u & 0 & 0 & a^2/\rho & 0 & a^2/\kappa & 0 \\ 0 & 0 & dl & r d\vartheta & 0 & 0 & 0 & 0 \\ 0 & 0 & w_l & w_u & 0 & a^2/\rho & 0 & a^2/\kappa \\ 0 & 0 & 0 & 0 & dl & r d\vartheta & 0 & 0 \\ 0 & 0 & 0 & 0 & 0 & 0 & w_l & w_u \\ 0 & 0 & 0 & 0 & 0 & 0 & dl & r d\vartheta \end{bmatrix}$$

$$B_j=\left[\frac{\partial w_l}{\partial l}, \frac{\partial w_l}{r\partial\vartheta}, \frac{\partial w_u}{\partial l}, \frac{\partial w_u}{r\partial\vartheta}, \frac{\partial\rho}{\partial l}, \frac{\partial\rho}{r\partial\vartheta}, \frac{\partial^s/c_v}{\partial l}, \frac{\partial^s/c_v}{r\partial\vartheta}\right]$$

$$C_i=\begin{bmatrix} -\frac{\rho w_l}{\cos\gamma}\left\{\sin\gamma\frac{\partial\gamma}{\partial l}+\frac{\partial\gamma}{\partial r}\right\} \\ dw_l-\frac{\partial w_l}{\partial r}(1-\tan\gamma)dr \\ \frac{\sin\gamma\{(w_u+u)^2+r\cdot f_{Sr}\}}{r}+2\sin\gamma\cos\gamma w_l^2\frac{\partial\gamma}{\partial l} \\ dw_u-\frac{\partial w_u}{\partial r}(1-\tan\gamma)dr \\ -w_r(w_u/r-2\omega) \\ d\rho-\frac{\partial\rho}{\partial r}(1-\tan\gamma)dr \\ -w_l\cos\gamma\frac{\partial(s/c_v)}{\partial r}(1-\tan\gamma) \\ d(s/c_v)-\frac{\partial(s/c_v)}{\partial r}(1-\tan\gamma)dr \end{bmatrix}=\begin{bmatrix} H_{\rho w} \\ dw_l-H_{w_l}dr \\ H_r \\ dw_u-H_{w_u}dr \\ H_u \\ d\rho-H_\rho dr \\ -w_l\cos\gamma H_s/dr \\ d(s/c_v)-H_s dr \end{bmatrix}$$

Acknowledgments

The presented results were achieved in a project, supported by the Deutsche Forschungsgemeinschaft in the scope of the "Sonderforschungsbereich 83." The research institute and the authors express their sincerest thanks for this promotion.

References

[1] Dettmering, W. and Becker, B., "Steps in the Development of a Supersonic Compressor Stage," AGARD-CP 34, Sept. 1968.

[2] Simon, H., "A Contribution to the Theoretical and Experimental Examination of the Flow Through Plane Supersonic Deceleration Cascades and Supersonic Rotors," *Journal of Engineering for Power*, Vol. 95, July 1973, pp. 233-243.

[3] Delaney, R. A. and Kavanagh, P., "Transonic Flow Analysis in Axial-Flow Turbomachinery Cascades by a Time-Dependent Method of Characteristics," *Transactions of the ASME, Journal of Engineering for Power*, Vol. 98, July 1976, pp. 356-364.

[4] Gopalakrishnan, S. and Bozzola, R., "A Numerical Technique for the Computation of Transonic Flows in Turbomachinery Cascades," ASME Paper 71-GT-42, 1971.

[5] Thompkins, W. T., "An Experimental and Computational Study of the Flow in a Transonic Compressor Rotor," Gas Turbine Laboratory Rept. 129, Cambridge, Mass., 1976.

[6] Erdos, J., Alzner, E., and Kalben, P.e.a., "Time Dependent Transonic Flow Solutions for Axial Turbomachinery," *Aerodynamic Analyses Requiring Advanced Computers*, NASA SP-347, 1975, pp. 587-622.

[7] Denton, J. D., "A Time Marching Method for Two and Three Dimensional Blade to Blade Flows," Marchwood Engineering Lab., Aeronautic Research Council Report R&M 3775, 1975.

[8] Rae, W. J., "Calculations of Three-Dimensional Transonic Compressor Flowfield by a Relaxation Method," AIAA Paper 77-199, 1977.

[9] Dodge, P. R. and Lieber, L. S., "Transonic 3-D Flow Analysis of Compressor Cascades with Splitter Vanes," AFAPL-TR-78-23, 1978.

[10] York, R. E. and Woodard, H. S., "Supersonic Compressor Cascades—An Analysis of the Entrance Region Flow Field Containing Detached Shock Waves," ASME Paper 75-GT-33, 1975.

[11] Prince, D. C., "Three-Dimensional Structures for Transonic/Supersonic/Compressor Rotors," AIAA Paper 79-0043, 1979.

[12] Wu, C. H., "A General Through-Flow Theory of Fluid Flow with Subsonic or Supersonic Velocity in Turbomachines of Arbitrary Hub and Casing Shapes," NACA TN 2302, 1951.

[13] Moeckel, W. E., "Approximate Method for Predicting Form and Location of Detached Shock Waves on Cones and Spheres," NACA TN 2000, 1950.

[14] Gallus, H. E., Bohn, D., and Broichhausen, K. D., "Measurements of Quasi-Steady and Unsteady Flow Effects in a Supersonic Compressor Stage," *Transactions of the ASME, Journal of Engineering for Power*, Vol. 99, Oct. 1977, pp. 537-544.

[15] Broichhausen, K. D. and Gallus, H. E., "Analysis of the Supersonic Unsteady Compressor Flow by Means of Semiconductor Probes and Visualization Techniques," *Proceedings of the Symposium on Measuring Techniques in Transonic and Supersonic Cascade Flow*, Central Electricity Research Laboratories RD/L/N 166/79, Feb. 1980, pp. 74-79.